International Journal of Bifurcation and Chaos, Vol. 18, No. 2 (2008) 481–494

A GALLERY OF OSCILLATIONS IN A RESONANT ELECTRIC CIRCUIT: HOPF-HOPF AND FOLD-FLIP INTERACTIONS

GUSTAVO REVEL*, DIEGO M. ALONSO† and JORGE L. MOIOLA‡
Instituto de Investigaciones en Ingeniería Eléctrica "Alfredo Desages",
Departamento de Ingeniería Eléctrica y de Computadoras,
Universidad Nacional de Sur,
Av. Alem 1253, (B8000CPB) Bahía Blanca, Argentina
CONICET
**grevel@uns.edu.ar*
†*dalonso@criba.edu.ar*
‡*jmoiola@criba.edu.ar*

Received November 27, 2006; Revised January 3, 2007

In this work, the dynamics of a coupled electric circuit is studied. Several bifurcation diagrams associated with the truncated normal form of the Hopf-Hopf bifurcation are presented. The bifurcation curves are obtained by numerical continuation methods. The existence of quasi-periodic solutions with two (2D torus) and three (3D torus) frequency components is shown. These, in certain way, are close (or have a tendency to end up) to chaotic motion. Furthermore, two fold-flip bifurcations are detected in the vicinity of the Hopf-Hopf bifurcation, and are classified correspondingly. The analysis is completed with time simulations, the continuation of several limit cycle bifurcations and the indication of resonance points.

Keywords: Bifurcations of periodic orbits; quasiperiodic solutions; double Hopf bifurcation; fold-flip bifurcation.

1. Introduction

The appearance of oscillations in physical systems may be explained, in several cases, by means of the Hopf bifurcation mechanism. In general, this phenomenon occurs when a pair of eigenvalues of the linearized system crosses the imaginary axis as a parameter of the system is varied. This kind of bifurcation has been widely studied in the literature (e.g. [Marsden & McCraken, 1976; Hassard *et al.*, 1981]), dealing with an important number of applications in real systems such as tethered satellites [Liaw & Abed, 1990], magnetic bearing systems [Mohamed & Emad, 1993], axial flow compressors [Gu *et al.*, 1999] and induction motors [Gordillo *et al.*, 2002], to mention only a few of them.

A situation with more dynamical complexity occurs when two pairs of eigenvalues cross the imaginary axis simultaneously at $\pm i\omega_1$ and $\pm i\omega_2$. Leading to the phenomenon known as Hopf-Hopf bifurcation (or double Hopf bifurcation), in addition to the typical emergence of periodic solutions from each single Hopf curve, a kind of interaction between the two oscillatory modes in certain regions of a two-parameter plane is present. When the ratio ω_1/ω_2 is irrational (nonresonant Hopf-Hopf bifurcation) the interaction gives birth to quasiperiodic motion known as two-dimensional or 2D torus. In certain cases, the Hopf-Hopf bifurcation gives rise to a more complex quasiperiodic motion called three-dimensional or 3D torus on which a third frequency that modulates the amplitude of the 2D torus oscillations is involved. Some applications with this kind of behavior have been reported very recently in the technical literature, particularly in mechanical

systems, such as in [Yu, 2002; Coller, 2003; Gattulli *et al.*, 2003; Chamara & Coller, 2004].

This work is focused on the dynamics of a simple, coupled electric circuit in which four typical bifurcation diagrams associated to the truncated normal form of the double Hopf singularity are glued together after varying a third parameter, by following the results described in [Kuznetsov, 1995]. This coupled electric circuit is a slight modification of the cubic model analyzed in [Itovich & Moiola, 2005] but, in the present case, a quadratic nonlinearity has been included. Three "simple" bifurcation diagrams are shown, comprising both Hopf curves, its corresponding Neimark–Saker bifurcations and, the 2D torus developing from them. Furthermore, a "complex" bifurcation diagram containing a 3D torus for certain combination of system parameters is obtained. The connection of these four diagrams seems to be didactic for assembling the big picture of the Hopf-Hopf bifurcation. Furthermore, a continuation of saddle-node bifurcations of cycles in the vicinity of the double Hopf degeneracy gives insights to locate other complex resonance points such as those special limit cycles with a double Floquet multiplier in +1, or a double Floquet multiplier in −1, or even the elusive degeneracy called *fold-flip* bifurcation containing one Floquet multiplier in +1 and one in −1. The latter singularity has been recently studied and reported in an extended type of Lorenz-84 model in [Kuznetsov *et al.*, 2004]. In the current coupled electric circuit, two *fold-flip* (FF) bifurcations have been detected in an isle of period-doubling bifurcations. This isle is located rather close to the double Hopf singularity, so more complex interactions would be expected after varying, appropriately, other system parameters. The appearance and deformation of the period-doubling island is outside the scope of the article. The interested readers can consult an equivalent phenomenon in an injected semiconductor laser in [Wieczorek *et al.*, 2001] and [Wieczorek *et al.*, 2005] or as a theoretical consequence of the appearance of period-doubling in strong resonance Hopf-Hopf bifurcation in the case $\omega_1/\omega_2 = 2$ (see [LeBlanc, 2000], for more details). In this paper we recovered the unfoldings of the FF singularity by numerical continuation using AUTO software and interpreted these results into the theoretical framework given by [Kuznetsov *et al.*, 2004]. It is also interesting to notice that the present analysis could be helpful when multiple double Hopf bifurcation points appear in the parameter space such as in delayed feedback systems (see, for example the Hopf bifurcation loops, Neimark–Sacker curves and period-doubling bifurcations in [Balanov *et al.*, 2005], using the Rössler system with delayed feedback).

This paper is organized as follows. In Sec. 2 some basic concepts of the truncated normal form of the Hopf-Hopf and the fold-flip bifurcations are reviewed. The analyzed circuit and its corresponding mathematical model are described in Sec. 3. In Secs. 4–6, the numerical results and a comparison between the normal form bifurcation diagrams are presented. Finally, some concluding remarks are expressed in Sec. 7.

2. Theoretical Background

In this section, a brief description of both Hopf-Hopf and fold-flip bifurcations normal forms is included. Most of this background material can be found in [Kuznetsov, 1995] and [Kuznetsov *et al.*, 2004], respectively.

Let us consider an n-dimensional smooth system depending on k parameters

$$\dot{x} = f(x, \mu), \tag{1}$$

where $x \in \mathbb{R}^n$, $\mu \in \mathbb{R}^k$ and $f : \mathbb{R}^n \to \mathbb{R}^n$ is a smooth function.

2.1. *Hopf-Hopf bifurcation*

Suppose that the linearization of (1) has two distinct pairs of purely imaginary eigenvalues for $x = 0$ and $\mu = 0$ with frequencies $\omega_1 > \omega_2$ and ω_1/ω_2 irrational. In addition assume that a reduction of the dynamics to the normal form is performed (see procedures, for example in [Guckenheimer & Holmes, 1993]). Then, considering that some nondegeneracy conditions hold and using polar coordinates (r_1, r_2, φ_1, φ_2), the truncated normal form of the Hopf-Hopf bifurcation is given by

$$\begin{aligned}
\dot{r}_1 &= r_1(\mu_1 + p_{11}r_1^2 + p_{12}r_2^2 + s_1 r_2^4),\\
\dot{r}_2 &= r_2(\mu_2 + p_{21}r_1^2 + p_{22}r_2^2 + s_2 r_1^4),\\
\dot{\varphi}_1 &= \omega_1,\\
\dot{\varphi}_2 &= \omega_2,
\end{aligned} \tag{2}$$

where $\mu_{1,2}$ are the bifurcation parameters, p_{jk} and s_k, $j, k = 1, 2$, are real coefficients. These coefficients and the frequencies $\omega_{1,2}$ depend on the parameters, but for simplicity this dependency is not indicated.

The last couple of equations in (2) corresponds to rotations over the planes $r_2 = 0$ and $r_1 = 0$ with

angular velocities ω_1 and ω_2, respectively. Since the first pair of equations is uncoupled from the second one, the bifurcation diagram is described by the following planar system, also known as *amplitude system*,

$$\begin{aligned} \dot{r}_1 &= r_1(\mu_1 + p_{11}r_1^2 + p_{12}r_2^2 + s_1 r_2^4), \\ \dot{r}_2 &= r_2(\mu_2 + p_{21}r_1^2 + p_{22}r_2^2 + s_2 r_1^4). \end{aligned} \tag{3}$$

Due to symmetry, it is enough to consider the cases where $r_{1,2} \geq 0$. The equilibrium point with $r_1 = r_2 = 0$ in (3), namely E_0, corresponds to a singular point of (2) located at the origin. The equilibrium points of (3) with $r_2 = 0$ or $r_1 = 0$, called E_1 and E_2 respectively, correspond to limit cycles of (2). The equilibrium E_3 with $r_{1,2} > 0$ corresponds to a 2D torus in the original system, while a limit cycle of (3) is a 3D torus of (2).

Depending on the signs of p_{11} and p_{22}, two different sets of bifurcation diagrams can be distinguished, namely simple cases ($p_{11} \cdot p_{22} > 0$) and complex cases ($p_{11} \cdot p_{22} < 0$). For simplicity, in Figs. 1–4 only those diagrams recognized in the model of the electric circuit analyzed in this paper are shown (the others can be seen in [Guckenheimer & Holmes, 1993] or [Kuznetsov, 1995]). Figures 1–3 correspond to simple cases and Fig. 4 to one of the complex cases. The associated phase portraits are shown surrounding the bifurcation diagrams, where the horizontal axis is proportional to r_1^2 and the vertical is to r_2^2. The origin represents the equilibrium E_0, the equilibria E_1 and E_2 lie on the coordinate axes, horizontal and vertical, respectively, and E_3 is depicted outside the axes. The filled dots indicate node equilibrium points, while the empty ones represent saddle equilibria.

The simple cases of Figs. 1–3 are obtained with $p_{11} < 0$ and $p_{22} < 0$, s_1 and s_2 can be set to

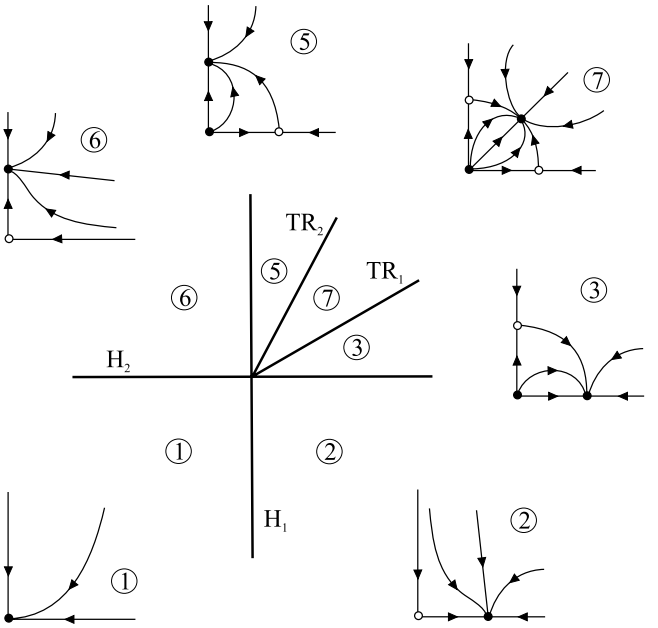

Fig. 2. Bifurcation diagram related to the truncated normal form of the Hopf-Hopf bifurcation for $p_{12} < 0$, $p_{21} < 0$ and $p_{12} \cdot p_{21} < p_{11} \cdot p_{22}$ ($p_{11} < 0,\ p_{22} < 0$).

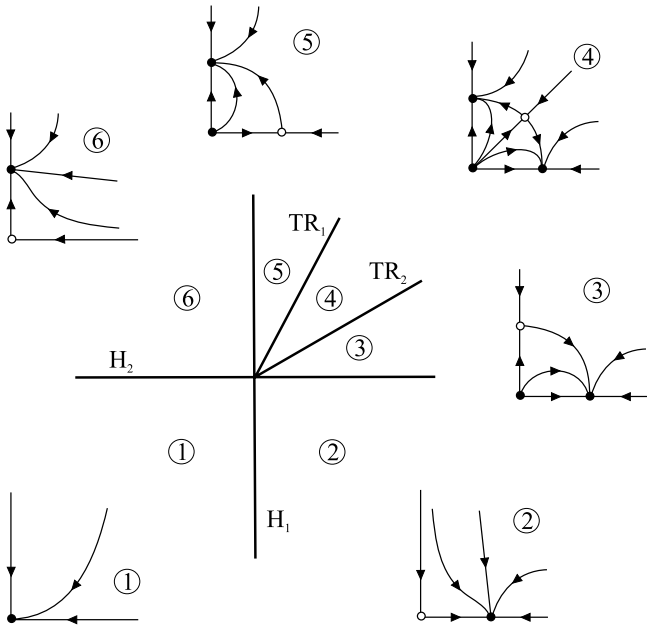

Fig. 1. Bifurcation diagram related to the truncated normal form of the Hopf-Hopf bifurcation for $p_{12} < 0$, $p_{21} < 0$ and $p_{12} \cdot p_{21} > p_{11} \cdot p_{22}$ ($p_{11} < 0,\ p_{22} < 0$).

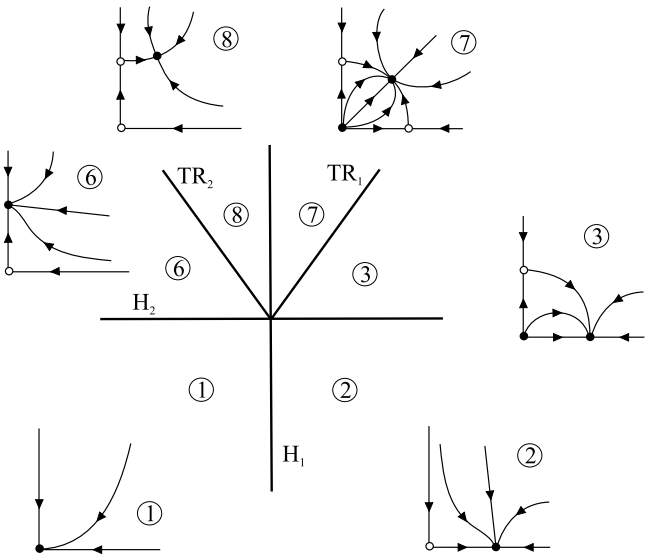

Fig. 3. Bifurcation diagram related to the truncated normal form of the Hopf-Hopf bifurcation for $p_{12} > 0$, $p_{21} < 0$ and $p_{12} \cdot p_{21} < p_{11} \cdot p_{22}$ ($p_{11} < 0,\ p_{22} < 0$).

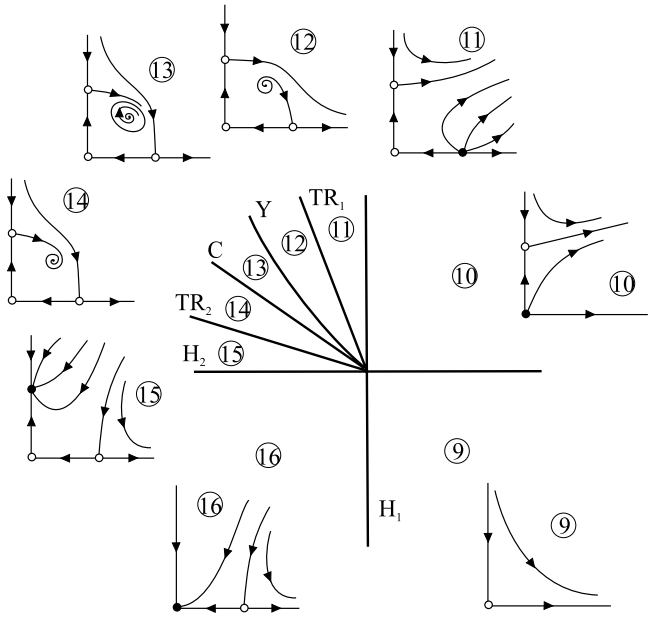

Fig. 4. Bifurcation diagram related to the truncated normal form of the Hopf-Hopf bifurcation for $p_{12} > 0$, $p_{21} < 0$ and $p_{12} \cdot p_{21} < p_{11} \cdot p_{22}$ ($p_{11} > 0,\ p_{22} < 0$).

$s_1 = s_2 = 0$ without changing the topology. Figure 1 is associated to the unfolding of (3) with $p_{12} < 0$, $p_{21} < 0$ and $p_{12} \cdot p_{21} > p_{11} \cdot p_{22}$. The equilibrium point E_0 is stable in region 1. It loses stability at H_1 when crossing to region 2, and a stable equilibrium E_1 appears. E_0 undergoes a second bifurcation on H_2 in the transition between regions 2 and 3, and another equilibrium E_2 arises. The equilibrium E_2 undergoes a bifurcation on TR_2 leading to E_3 in region 4. This equilibrium collapses with E_1 on TR_1 and disappears (region 5). Then E_1 vanishes on H_1 (region 6). Finally, E_2 collapses at H_2 (region 1). The situation of Fig. 2, is rather similar, but the curves TR_1 and TR_2 are swapped and then phase portrait 4 is replaced by diagram 7. In this case $p_{12} < 0$, $p_{21} < 0$ and $p_{12} \cdot p_{21} < p_{11} \cdot p_{22}$. Figure 3 corresponds to $p_{12} > 0$, $p_{21} < 0$ and $p_{12} \cdot p_{21} < p_{11} \cdot p_{22}$. The difference from Fig. 2 is that TR_2 crossed to the left of H_1. The new phase portrait is labeled with 8 in Fig. 3.

The complex case ($p_{11} \cdot p_{22} < 0$) of Fig. 4 is obtained with $p_{11} > 0$, $p_{22} < 0$, $p_{12} > 0$, $p_{21} < 0$ and $p_{12} \cdot p_{21} < p_{11} \cdot p_{22}$ (restrictions on s_1 and s_2, as well as nondegeneracy conditions, can be seen in [Kuznetsov, 1995]). The equilibria E_0, E_1 and E_2 suffer similar bifurcations as in the simple cases, but E_3 undergoes a Hopf bifurcation at the curve C. The emerging limit cycle vanishes at an heteroclinic bifurcation depicted by the curve Y. This scenario cannot occur in the simple cases.

Bifurcation diagrams of the amplitude system (3) can be related to the four-dimensional system (2) as follows. The curves H_1 and H_2 correspond to Hopf bifurcations of the origin of (2). The point $(\mu_1, \mu_2) = (0, 0)$, where H_1 and H_2 occur simultaneously, is the Hopf-Hopf bifurcation. The curves TR_1 and TR_2 represent bifurcations of limit cycles (E_1 and E_2) into 2D torus, i.e. Neimark–Saker bifurcations. In the complex case, the Hopf bifurcation of the equilibrium E_3 determines the birth of a 3D torus.

Although a four-dimensional generic system with higher order terms than those considered in (2) is never topologically equivalent to the system given by the truncated normal form, it provides information about the behavior of the complete system [Kuznetsov, 1995]. The electric circuit considered in this work develops, for different values of the parameters, the four dissimilar bifurcation diagrams shown in Figs. 1–4.

2.2. *Fold-flip bifurcation*

Assume that (1) undergoes simultaneously a saddle node bifurcation of periodic orbits and a period doubling bifurcation, i.e. a fold-flip bifurcation for some $\mu = 0$ near $x = 0$. Suppose that a Poincaré map at this point is obtained. Then performing a reduction to the center manifold and neglecting higher order terms (see the procedure in [Kuznetsov *et al.*, 2004]), the dynamics of (1) in the neighborhood of $x = 0$ and $\mu = 0$ can be studied by means of the truncated normal form of the fold-flip bifurcation given by the map $N : \mathbb{R}^2 \times \mathbb{R}^2 \to \mathbb{R}^2$

$$z \mapsto N(z, \mu), \quad z = (z_1, z_2)^T, \quad \mu = (\mu_1, \mu_2)^T,$$

$$N(z, \mu) = \begin{pmatrix} \mu_1 + (1 + \mu_2) z_1 + \frac{1}{2} a z_1^2 + \frac{1}{2} b z_2^2 + \frac{1}{6} c z_1^3 + \frac{1}{2} d z_1 z_2^2 \\ -z_2 + z_1 z_2 \end{pmatrix}, \tag{4}$$

where μ_1 and μ_2 are the bifurcation parameters, a, b, c and d, are coefficients that may depend smoothly on the parameters μ. Notice that fixed points of (4) and the associated bifurcations correspond to cycles

of (1) and their bifurcations. Local bifurcations of fixed points (fold, flip and Neimark–Sacker) can be studied by considering the map (4). Nevertheless, to study global bifurcations it is suitable to approximate (4) by the unit shift of a vector field as [Kuznetsov *et al.*, 2004]

$$RN(z,\mu) = \varphi^1(z,\mu) + O(\|\mu\|^2) + O(\|z\|^2\|\mu\|) + O(\|z\|^4), \tag{5}$$

where $R = \left(\begin{smallmatrix} 1 & 0 \\ 0 & -1 \end{smallmatrix}\right)$, and $\varphi^t(z,\mu)$ is the flow generated by the system

$$\begin{aligned} \dot{z}_1 &= \mu_1 + \left(-\frac{1}{2}a_0\mu_1 + \mu_2\right) z_1 + \frac{1}{2}a_0 z_1^2 + \frac{1}{2}b_0 z_2^2 \\ &\quad + d_1 z_1^3 + d_2 z_1 z_2^2, \\ \dot{z}_2 &= \frac{1}{2}\mu_1 z_2 - z_1 z_2 + d_3 z_1 z_2^2 + d_4 z_2^3, \end{aligned} \tag{6}$$

where $a_0 = a(0)$, $b_0 = b(0)$, $c_0 = c(0)$ and $d_0 = d(0)$ denote the critical values ($\mu_1 = \mu_2 = 0$) of the coefficients of the truncated normal form, and

$$\begin{aligned} d_1 &= \frac{1}{6}\left(c_0 - \frac{3}{2}a_0^2\right), \\ d_2 &= \frac{1}{2}\left(d_0 + \frac{1}{2}b_0(2 - a_0)\right), \\ d_3 &= \frac{1}{4}(a_0 - 2), \\ d_4 &= \frac{1}{4}b_0. \end{aligned}$$

Bifurcations of the truncated normal form can be explained by studying bifurcations of the vector field (6). Let us describe only those bifurcation diagrams that will be present in the numerical analysis of the electric circuit considered in this paper. These diagrams are given in Figs. 5 and 6 for $a_0 > 0$ and $a_0 < 0$, respectively ($b_0 < 0$, $c_0 = d_0 = 1$). The curves labeled $F^{\pm}$ and $PD^{\pm}$ denote fold and flip bifurcation curves, respectively. The phase portraits included in Figs. 5 and 6 represent schematically the trajectories of the map by a continuous curve. It is worth to mention that the true orbits must consider the reflection R in (5) and actually it alternates between the upper and lower half phase planes. The points on the z_1 (horizontal) axis are fixed points of the map and that in the upper half plane is a period-two fixed point. Node and focus fixed points are represented by filled circles and saddle points by empty circles.

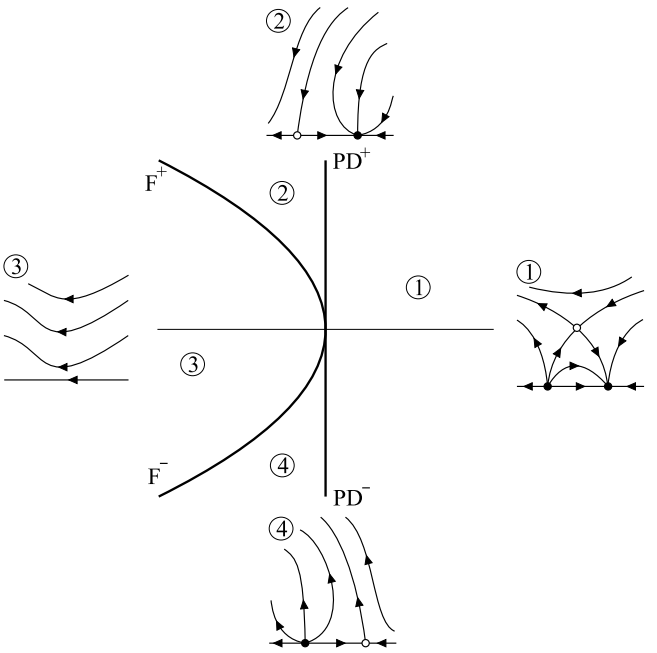

Fig. 5. Unfolding of the fold-flip bifurcation for the case $a_0 < 0$, $b_0 < 0$ and $c_0 = d_0 = 1$.

The first unfolding is obtained with $a_0 < 0$, and is depicted in Fig. 5. In region 1 there are three fixed points, a stable and an unstable node on the z_1 axis; and a period-two saddle. This period-two point does not appear in region 2 because of the period doubling bifurcation PD^+, and the unstable node is transformed into a saddle. This saddle

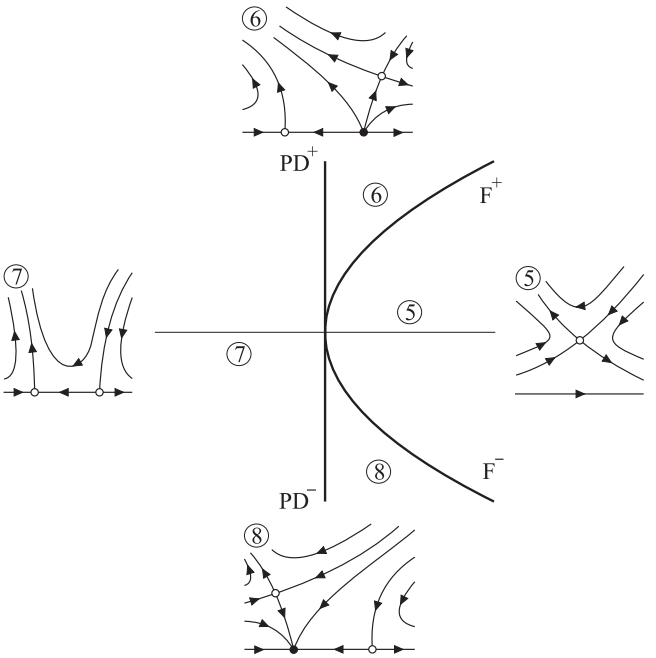

Fig. 6. Unfolding of the fold-flip bifurcation for the case $a_0 > 0$, $b_0 < 0$ and $c_0 = d_0 = 1$.

collapses with the stable node and both disappear when crossing to region 3 due to the fold bifurcation curve F^+. On region 4, an unstable node and a saddle point do appear because of the fold curve F^-. The saddle point bifurcates into a stable node when crossing the curve PD^- back into region 1 and a period-two fixed point is created.

The second case is shown in Fig. 6, where $a_0 > 0$. In region 5 only a period-two saddle fixed point exists. Crossing the curve F^+ against region 6, two equilibria on the horizontal axis do appear, a saddle and an unstable node that it is connected with the period-two point. Crossing PD^+ from region 6 to 7, the unstable period-two point vanishes and the unstable node becomes a saddle. The other saddle point undergoes a period doubling bifurcation at PD^-, becoming into a stable node and leading to a period-two point in region 8. This stable node collides with the saddle equilibrium when crossing the curve F^- and only the period-two point exists in region 5.

3. Case Study: A Nonlinear Electric Circuit

Let us consider the circuit shown in Fig. 7. Defining variables $v_{C_1} = x_1$, $i_{L_1} = x_2$, $v_{C_2} = x_3$, and $i_{L_2} = x_4$, $C_1 = 1/\eta_1$, $R = \eta_2$, $\alpha = \eta_3/\eta_1$, $C_2 = 1/(1+\sqrt{2})$, $L_1 = \sqrt{2}$, $L_2 = 1/(2-\sqrt{2})$, and characterizing the nonlinear resistance by the relation $i_G = -(1/2)v_G - \alpha_2 v_G^2 + \alpha_3 v_G^3$, with α_2 and α_3 constants, the model of the system is given by

$$\begin{aligned}
\dot{x}_1 &= \eta_1\left(\frac{1}{2}x_1 + x_2 - x_4 - \alpha_2 x_1^2 - \alpha_3 x_1^3\right) + \eta_3 x_2,\\
\dot{x}_2 &= -\frac{1}{L_1}x_1,\\
\dot{x}_3 &= \frac{1}{C_2}x_4,\\
\dot{x}_4 &= \frac{1}{L_2}\left(x_1 - x_3 - \eta_2 x_4\right).
\end{aligned} \tag{7}$$

This circuit has been inspired in a similar model analyzed in [Yu, 2002]. However, in this case, the controlled current source (αi_{L_1}) introduces resonances when parameter η_3 is varied [Itovich & Moiola, 2005] and then transition from nonresonant to resonant Hopf-Hopf bifurcations can be obtained. Similar scenarios can be recovered by setting $1/L_1$ as a free parameter with $\alpha = 0$, i.e. without the controlled current source.

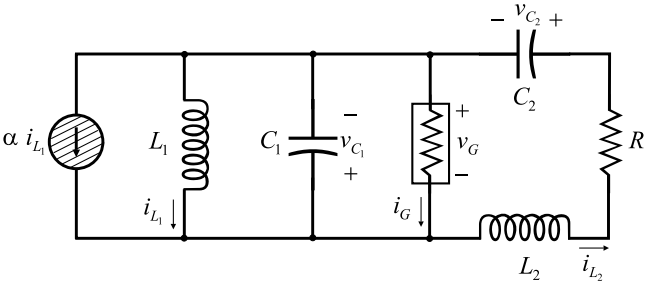

Fig. 7. Electric circuit of the coupled oscillator.

System (7) has a unique equilibrium point at the origin $x_1 = x_2 = x_3 = x_4 = 0$. It is easy to verify that when $\eta_1 = 2 - \eta_3$ and $\eta_2 = (1+(\sqrt{2}/2))(1 - (1/2)\eta_3)$ the system linearization around the equilibrium point has two pairs of imaginary eigenvalues $\lambda_{1,2} = \pm j\omega_1$ and $\lambda_{3,4} = \pm j\omega_2$ with $\omega_{1,2} = \sqrt{\gamma \mp \sqrt{-2+\gamma^2}}$, and $\gamma = (1/2)[3 - (1-\sqrt{2})\eta_3 - (1/4)\eta_3^2]$. This is a necessary condition to have a Hopf-Hopf bifurcation. Notice that when $\eta_3 = -6 + 4\sqrt{2} \cong -0.3431$ both frequencies are coincident $\omega_{1,2} = 2^{\frac{1}{4}}$, and a resonant 1:1 Hopf-Hopf bifurcation occurs.

4. Local Analysis of the Hopf-Hopf Bifurcation

In this section, the nonresonant Hopf-Hopf bifurcation is studied by means of numerical continuation methods. Bifurcation diagrams in the parameter plane η_1–η_2 are obtained for different values of η_3, namely $\eta_3 = 0$, -0.075, -0.140 and -0.220. As will be shown next, parameter η_3 allows traveling between different bifurcation diagrams associated to the normal form of the Hopf-Hopf bifurcation. Parameters $\alpha_{2,3}$ are fixed at $\alpha_2 = 0.6$ and $\alpha_3 = 1$.

4.1. *Case a*

The bifurcation diagram for $\eta_3 = 0$ is shown in Fig. 8. This diagram is analogous to the scheme of Fig. 1 except for the rotation on the curves. The different phenomena associated with the bifurcation diagram shown in Fig. 8 and the corresponding phase portraits displayed in Fig. 1, are described below. Within region 1 the origin is a stable equilibrium point, and making a counterclockwise round trip, first the equilibrium becomes unstable at H_1 and a stable limit cycle is created (region 2). In region 3, a second (unstable) limit cycle that emerges from the origin at the Hopf bifurcation

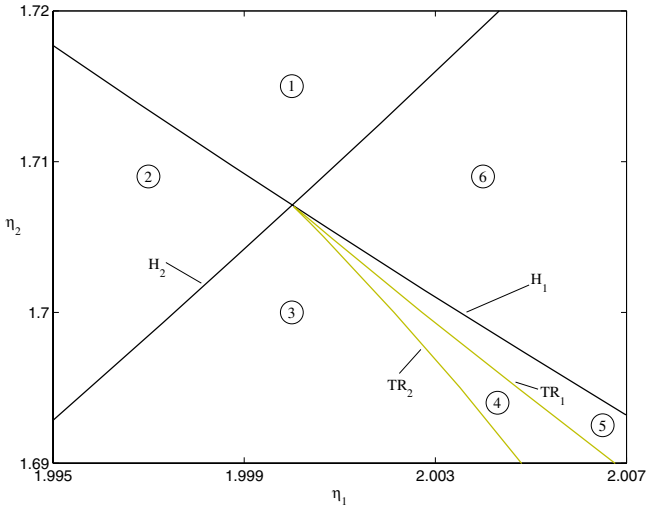

Fig. 8. Bifurcation diagram for $\eta_3 = 0$ ($\alpha_2 = 0.6$ and $\alpha_3 = 1$).

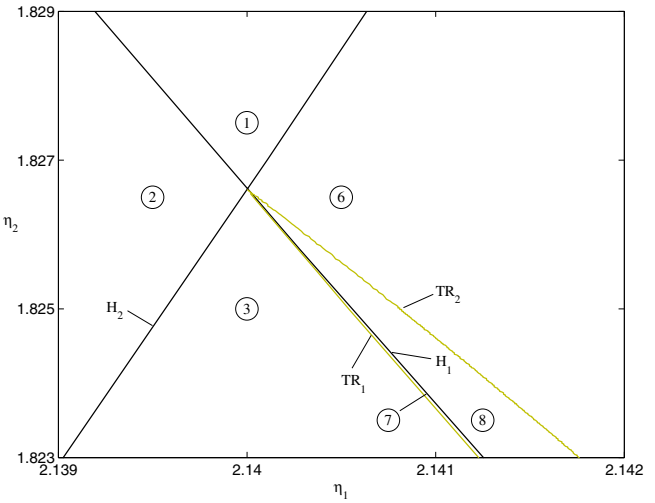

Fig. 10. Bifurcation diagram for $\eta_3 = -0.140$ ($\alpha_2 = 0.6$ and $\alpha_3 = 1$).

H_2 coexists. The unstable cycle becomes stable because of the Neimark–Sacker bifurcation TR_2 and an unstable 2D torus arises (region 4). This torus collapses at a second Neimark–Sacker bifurcation TR_1, and in region 5 only two limit cycles, one stable and the other unstable, are present. The unstable cycle vanishes at H_1 (region 6) and the stable one disappears at H_2 (region 1).

4.2. *Case b*

Fixing $\eta_3 = -0.075$, the bifurcation diagram shown in Fig. 9 is obtained. This case corresponds to the schematic diagram represented in Fig. 2. The qualitative change respect to the case described before is the swap between the Neimark–Sacker curves TR_1 and TR_2 (cf. Fig. 1). For this reason, when crossing from region 3 to region 7, the stable cycle becomes unstable and a stable 2D torus is created at TR_1. This torus collapses at the curve TR_2 and the unstable cycle created in H_2 becomes stable (region 5). The dynamics on the remaining regions is analogous to the case $\eta_3 = 0$.

4.3. *Case c*

The continuation results for $\eta_3 = -0.140$ are represented in Fig. 10. The corresponding schematic diagram is shown in Fig. 3. Notice that the Neimark–Sacker curve TR_2 overpasses the Hopf curve H_1. Remember that in region 7 the origin

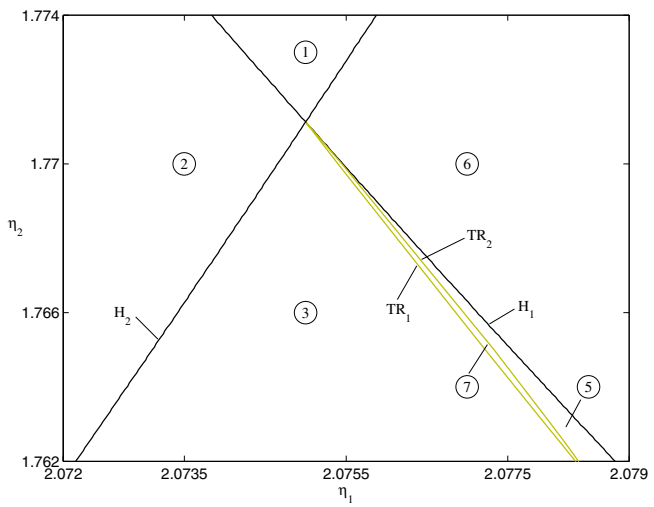

Fig. 9. Bifurcation diagram for $\eta_3 = -0.075$ ($\alpha_2 = 0.6$ and $\alpha_3 = 1$).

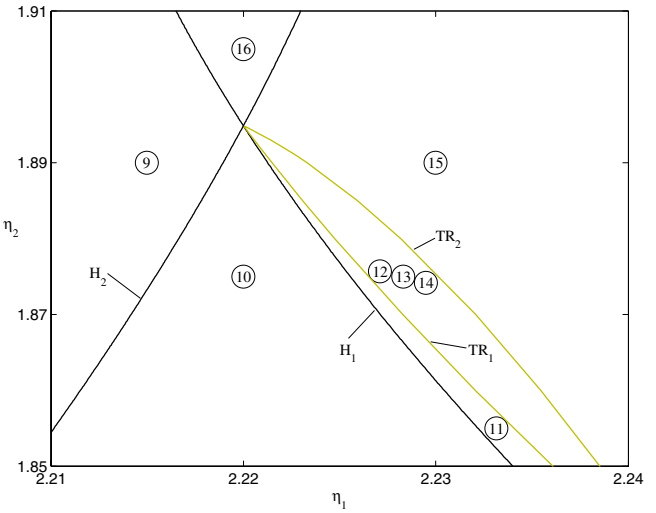

Fig. 11. Bifurcation diagram for $\eta_3 = -0.220$ ($\alpha_2 = 0.6$ and $\alpha_3 = 1$).

is unstable, and there is a pair of unstable limit cycles and a stable 2D torus. In region 8 only one of these cycles survives, since the other collapses at the Hopf bifurcation H_1. Finally, the 2D torus vanishes at the TR_2 bifurcation and the cycle becomes stable (region 6).

4.4. *Case d*

The bifurcation diagram displayed in Fig. 11 is obtained by fixing $\eta_3 = -0.220$, and can be related to the schematic diagram in Fig. 4. In this case, the dynamical scenario is more complicated than the previous one and corresponds to the complex cases of the truncated normal form including bifurcations of torus (curves Y and C in Fig. 4). To begin, it is worth to mention that the Neimark–Sacker curve TR_1 also overpasses the curve H_1, when considering its transition from case c described before. However a substantial difference from the previous case is the sign of the stability index of the Hopf bifurcation H_1. In cases (a)–(c) the cycle born at H_1 arises

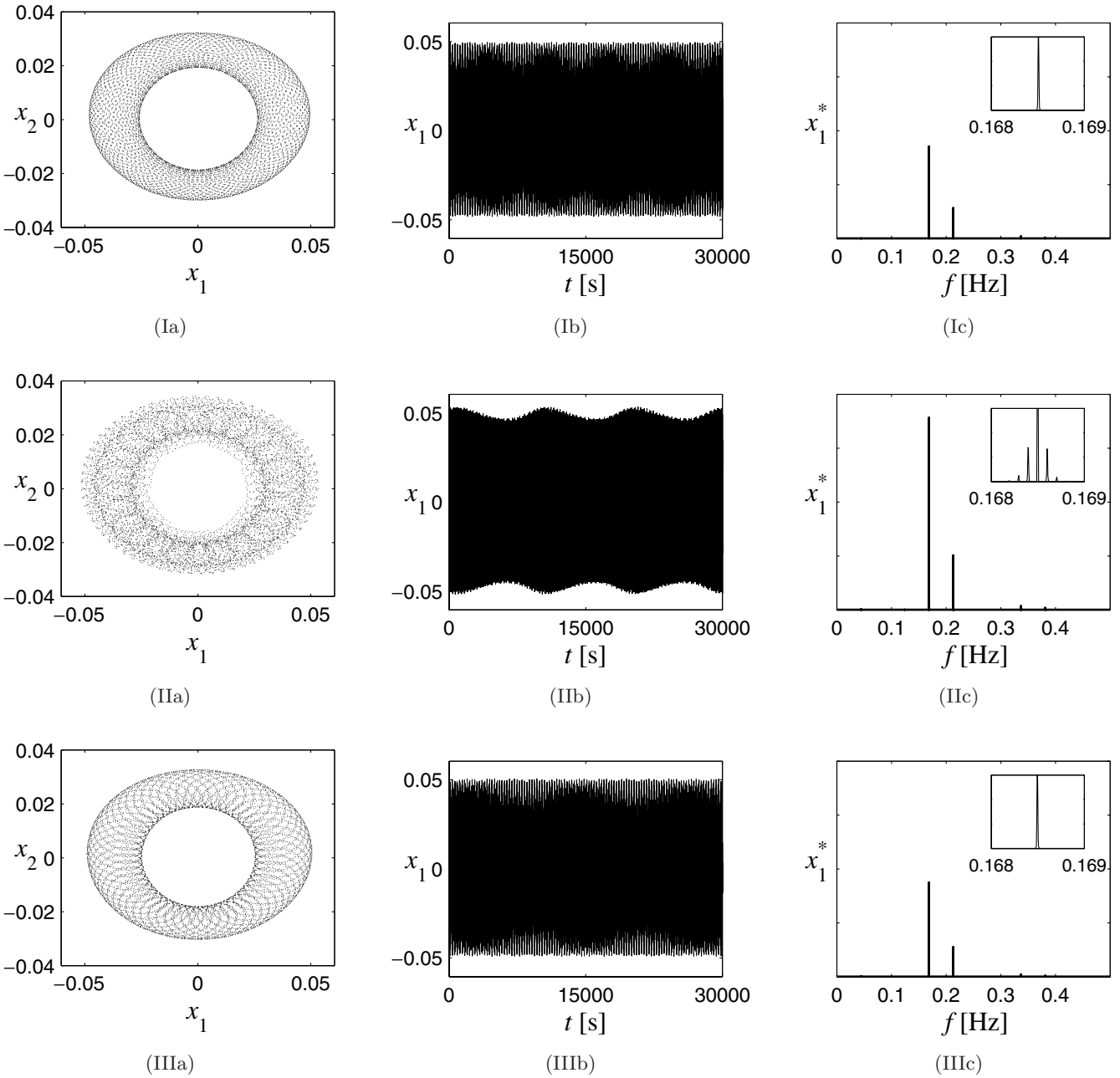

Fig. 12. (I) Unstable 2D torus in region 12. (II) Stable 3D torus present in region 13. (III) Stable 2D torus located in region 14.

to the left of the curve, it is stable on the upper segment of the curve (above the Hopf-Hopf bifurcation) and unstable on the lower part. In the present case, the cycle emerges towards the right of H_1 and it is unstable all over the curve (in the range shown in Fig. 11). This situation produces a complete change in the associated phase portraits and it is described below.

In region 9, the equilibrium is unstable and it is locally the unique limit set. In region 10 an unstable limit cycle generated by the Hopf bifurcation H_2 coexists with the equilibrium. A second unstable limit cycle is created by means of H_1 describing the scenario of region 11. The Neimark–Sacker bifurcation TR_1 creates an unstable 2D torus in region 12 (see in Fig. 12(Ia) a projection over the plane x_1–x_2). Bifurcation curves Y and C, actually present in the truncated normal form (see Fig. 4), are not shown in Fig. 11 since the implemented algorithms on the numerical continuation package do not compute bifurcations of torus.[1] Nevertheless, several simulations have been made in order to corroborate the existence of the limit sets associated to regions 12–14. The unstable 2D torus of region 12 suffers a heteroclinic bifurcation (curve Y in Fig. 4) leading to a stable 3D torus (region 13). A projection of the 3D torus over the plane x_1–x_2 with $\eta_1 = 2.222220$ and $\eta_2 = 1.888$ is shown in Fig. 12(IIa). The 3D torus collapses for increasing values of η_1 (curve C in Fig. 4) and in region 14 the 2D torus is stable. This situation is illustrated in Fig. 12(IIIa), for $\eta_1 = 2.222225$ and $\eta_2 = 1.888$. Subsequently the torus collapses on the Neimark–Sacker bifurcation TR_2 and one of the unstable cycles becomes stable (region 15). This cycle disappears at the Hopf bifurcation H_2, and the equilibrium at the origin turns stable (region 16). Crossing the curve H_1, the scenario returns to the starting place (region 9).

Temporal signals (second column) and their corresponding frequency spectra (third column) are shown in Figs. 12(Ib)–(IIIb), and Figs. 12(Ic)–(IIIc), respectively. Although the three cases reveal the existence quite distinguishably of two frequencies or modes at $f_1 \cong 0.1285$ Hz and $f_2 \cong 0.2130$ Hz, it is clear that the signal of the 3D torus presents an amplitude modulation [Fig. 12(IIb)] that is observable on the spectrum because of the appearance of frequency components near f_1 and f_2 (see the rectangles in Figs. 12(Ic)–(IIIc)). This third frequency is approximately $f_3 \cong 0.0001$ Hz.

5. Complex Unfolding in Detail

As mentioned before, the mechanism that turns the "simple" Hopf-Hopf bifurcation unfolding (case c) into the "complex" one (case d) is the vanishing of the stability index of the Hopf bifurcation curve H_1. Remember that in case c ($\eta_3 = -0.140$), H_1 develops a cycle to its left while in case d ($\eta_3 = -0.220$), H_1 generates a cycle to its right, at least in the neighborhood of the Hopf-Hopf point. Let us now describe briefly the mechanism. For $\eta_3 < -0.140946$ a pair of generalized Hopf bifurcation points, namely GH_1 and GH_2, do appear (actually these points collide for $\eta_3 = -0.140946$ and disappear for greater values of η_3). This scenario is depicted schematically in Fig. 13(a). The dashed segment between GH_1 and GH_2 corresponds to a generation of an unstable limit cycle to the right

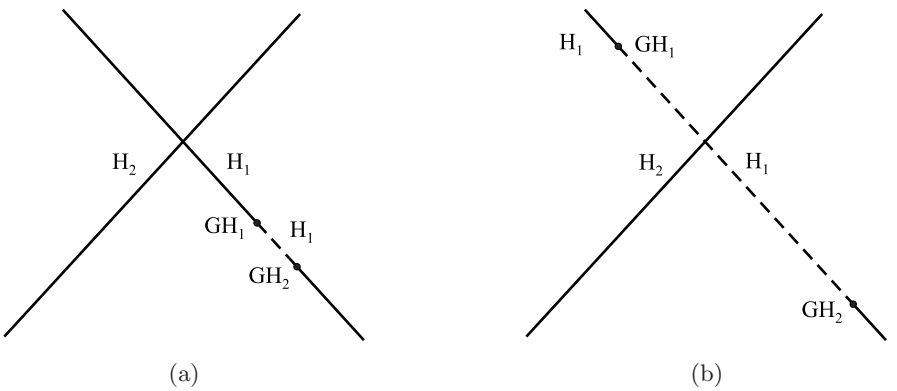

Fig. 13. Schematic representation of a mechanism that turns the "simple" cases of the unfolding of the Hopf-Hopf bifurcation into "complex".

[1]Actually, this is a difficult task and the readers are referred to a recent contribution of Schilder *et al.* [2006] for computing the continuation of the torus and detecting its bifurcations.

of H_1. For $\eta_3 \cong -0.14965$ the point GH_1 coincides with the Hopf-Hopf point and for $\eta_3 < -0.14965$ the situation is that shown in Fig. 13(b). In this case the Hopf bifurcation H_1 creates an unstable cycle to its right in the neighborhood of the Hopf-Hopf point leading to the complex case.

5.1. *Global bifurcation analysis for* $\eta_3 = -0.220$

The vanishing of the stability index of H_1 is related to a global phenomenon involving connections of cyclic fold bifurcation curves. In order to analyze these interactions a numerical analysis on a larger region of the parameter plane η_1–η_2 for $\eta_3 = -0.220$ is performed. The bifurcation diagram is displayed in Fig. 14. The labels and colors used on the figures are shown in Table 1, the super/sub indexes on each individual label are used to distinguish the curves.

The generalized Hopf bifurcation GH_1 is located at $\eta_1 = 2.21033$ and $\eta_2 = 1.96332$, this point divides the Hopf bifurcation curve in two [see Fig. 15(a)]. Therefore, the cycle emerging from this curve is stable above the singularity GH_1, and unstable below it. In addition, a cyclic fold branch F_1^a emerges form GH_1, as indicated by the normal form of the generalized Hopf bifurcation [Kuznetsov, 1995]. This branch ends in a cusp point

Table 1. Labels and colors used in the figures.

Bifurcation	Label	Color
Hopf	H	black
Generalized Hopf	GH	blue dot
Cyclic fold	F	blue
Neimark–Sacker	TR	ocher
Period doubling	PD	red
Cusp	C	—
Resonances	R	red dot
Fold-Flip	FF	black dot

C_1, with the cyclic fold F_1^b. The second generalized Hopf bifurcation GH_2 [see Fig. 15(b)] is situated at $\eta_1 = 2.37169$ and $\eta_2 = 1.63224$. The scenario is similar to the preceding case; GH_2 divides the Hopf branch in two. Both branches give birth to unstable cycles, but in the upper segment the cycle grows to the right and in the lower to the left. The cyclic fold F_1^c emerges from GH_2 and coalesces with F_1^d at the cusp point C_2.

Let us now describe the global phenomena connecting GH_1 and GH_2 depicted in Fig. 14. Starting from GH_1, the cyclic fold curve F_1^a forms the cusp point C_1 with F_1^b [Fig. 15(a)], also F_1^b forms the cusp point C_3 with the cyclic fold branch F_2. This curve ends in another cusp point C_4 along with the cyclic fold F_3. The cusp point C_5 connects the

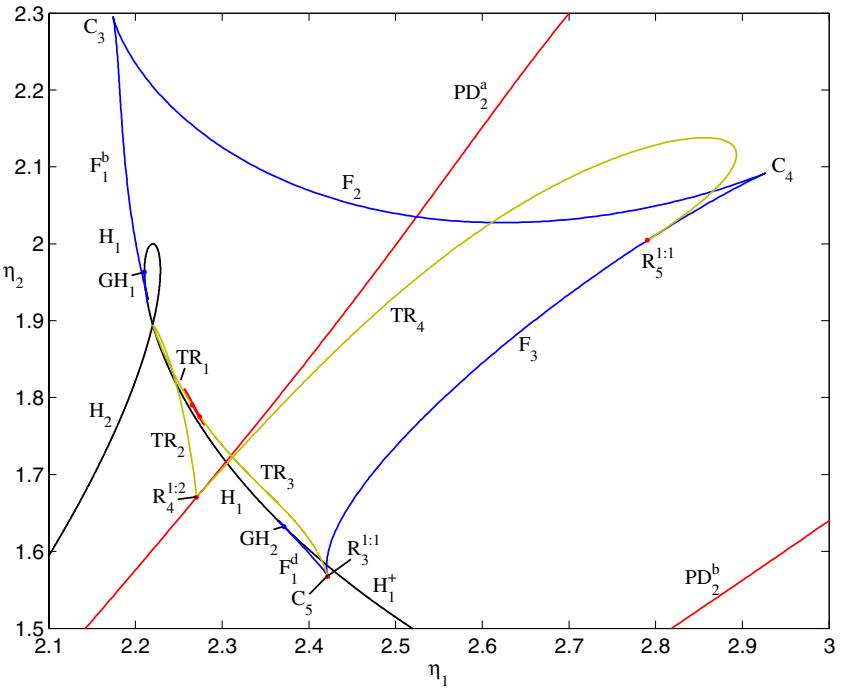

Fig. 14. Bifurcation diagram for $\eta_3 = -0.220$, including global phenomena.

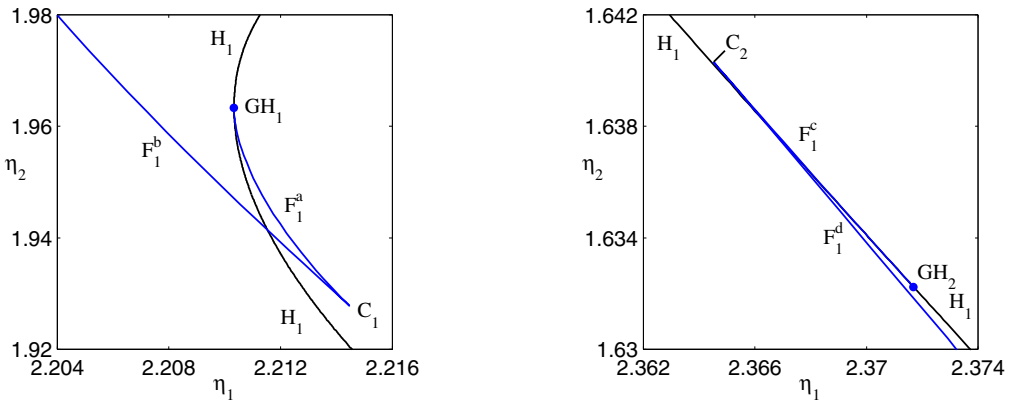

(a) (b)

Fig. 15. Generalized Hopf bifurcations along the branch H_1 ($\eta_3 = -0.220$).

curves F_3 with F_1^d, C_2 joins F_1^d with F_1^c, and the last one ends at the generalized Hopf bifurcation GH_2 [Fig. 15(b)]. This particular structure of cyclic fold curves along with a closed curve of period doubling bifurcations plays an important role in the dynamic of the system for increasing values of η_3. This interaction leads to fold-flip bifurcations and will be explained in the next section.

Following the description of Fig. 14, let us consider the detailed diagram of Fig. 16. The Neimark–Sacker bifurcation TR_1 born at the Hopf-Hopf bifurcation point, ends on a closed curve of period doubling bifurcations PD_1. The $1:2$ resonance point $R_1^{1:2}$ (two Floquet's multipliers at -1), is located at $\eta_1 = 2.26559$ and $\eta_2 = 1.79021$. A second 1:2 resonance point on PD_1, namely $R_2^{1:2}$, at $\eta_1 = 2.27452$ and $\eta_2 = 1.77531$ is detected. A Neimark–Sacker bifurcation TR_3 is originated from this point. This bifurcation curve ends in the 1:1 resonance point $R_3^{1:1}$ (two multipliers at 1) on the cyclic fold curve F_3, at $\eta_1 = 2.42222$ and $\eta_2 = 1.56755$. A homoclinic branch and its tangent curves are expected to be found near this point. The study of the system dynamics near these resonance points is beyond the scope of this work, and they are only mentioned for the sake of completeness.

There are two other curves of period doubling bifurcations in Fig. 14. In this case, the bifurcations

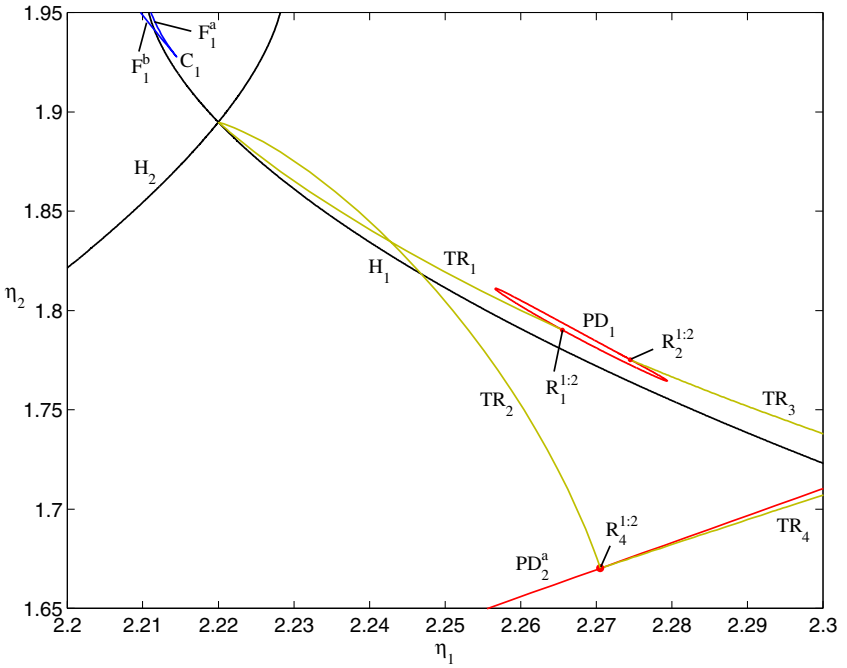

Fig. 16. Expanded view of the bifurcation diagram for $\eta_3 = -0.220$.

are originated from the Hopf cycle H_2 and they are represented by the curves PD_2^a and PD_2^b. In addition, these curves also form a closed curve of period doubling bifurcations, that it is much larger than the previous (the complete island is not shown in Fig. 14). There is a 1:2 resonant point $R_4^{1:2}$ at $\eta_1 = 2.27059$ and $\eta_2 = 1.67033$ over the curve PD_2^a. This point is connected by means of the Neimark–Sacker bifurcation TR_4, with a 1:1 resonant point $R_5^{1:1}$ on the cyclic fold curve F_3 at $\eta_1 = 2.79074$ and $\eta_2 = 2.00461$. As mentioned for $R_3^{1:1}$, a homoclinic branch is expected to emanate from this point.

6. Fold-Flip Bifurcations

The closed curve of period doubling bifurcations interacts with a fold bifurcation structure leading to a couple of fold-flip bifurcation points for $\eta_3 = -0.140$. The global scenario is depicted in Fig. 17. The singularities GH_1 and GH_2 no longer exist for $\eta_3 > -0.140946$, so the four branches of cyclic fold curves F_1^a, F_1^b, F_1^c and F_1^d now form a single and continuous curve named F_1. In addition, the curve H_1 generates a limit cycle to the left: above the Hopf-Hopf bifurcation the oscillation is stable and below the singularity it is unstable. This is the main difference when comparing to the bifurcation diagram of Fig. 14, besides the change in the local unfolding of the Hopf-Hopf bifurcation. It is worth to mention that the isle of period doubling bifurcations PD_1 is now located below H_1. The interactions of this isle and the fold curve are difficult to be noticed, even in the corresponding blow up of Fig. 17. Toward this end a schematic representation is given in Fig. 18(a). The remaining curves and resonance points are similar to the preceding case.

The fold-flip bifurcation point FF_1 is at $(\eta_1, \eta_2) = (2.173411, 1.748704)$ and FF_2 at $(\eta_1, \eta_2) = (2.184536, 1.728625)$. The schematic representations of both fold-flip bifurcations are shown in Figs. 18(b) and 18(c). The curves are labeled in correspondence to the names of Fig. 17. The dynamical scenario on a neighborhood of the bifurcation point FF_1 [Fig. 18(b)] is associated to the unfolding of the truncated normal form of the fold-flip bifurcation displayed in Fig. 5. In region 1 there exist an unstable period doubling orbit and two limit cycles, a stable one and a saddle type cycle. The period-2 cycle coalesces with the saddle limit cycle at PD_1^+, therefore, in region 2 only the stable and the saddle limit cycles do exist. This situation holds until the curve F_1^+ is reached, where both cycles collapse and disappear, hence, there are no orbits in region 3. An unstable limit cycle and a saddle cycle are created by the cyclic fold bifurcation F_1^- and they are present in region 4. The unstable limit cycle suffers

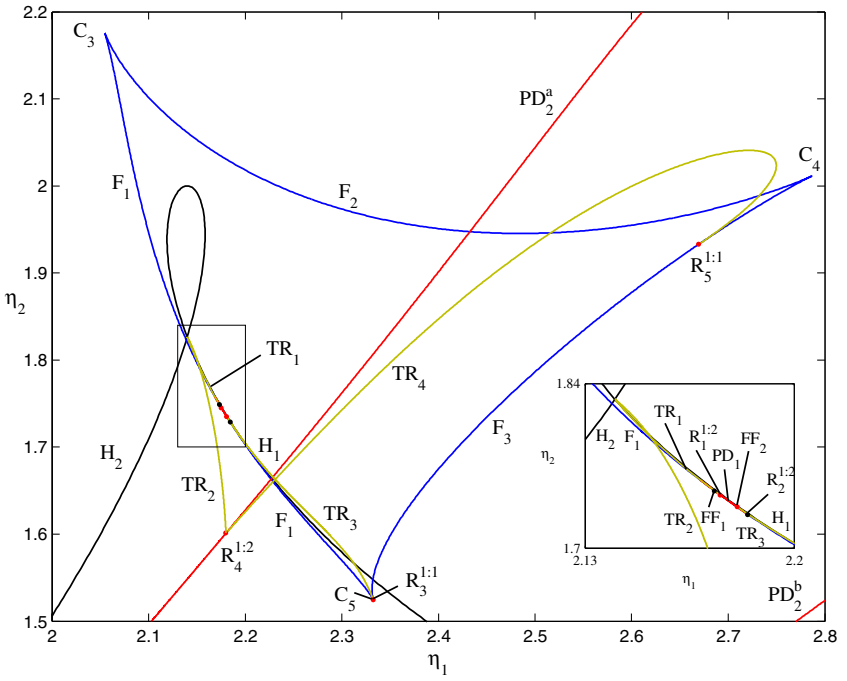

Fig. 17. Bifurcation diagram for $\eta_3 = -0.140$, including global phenomena.

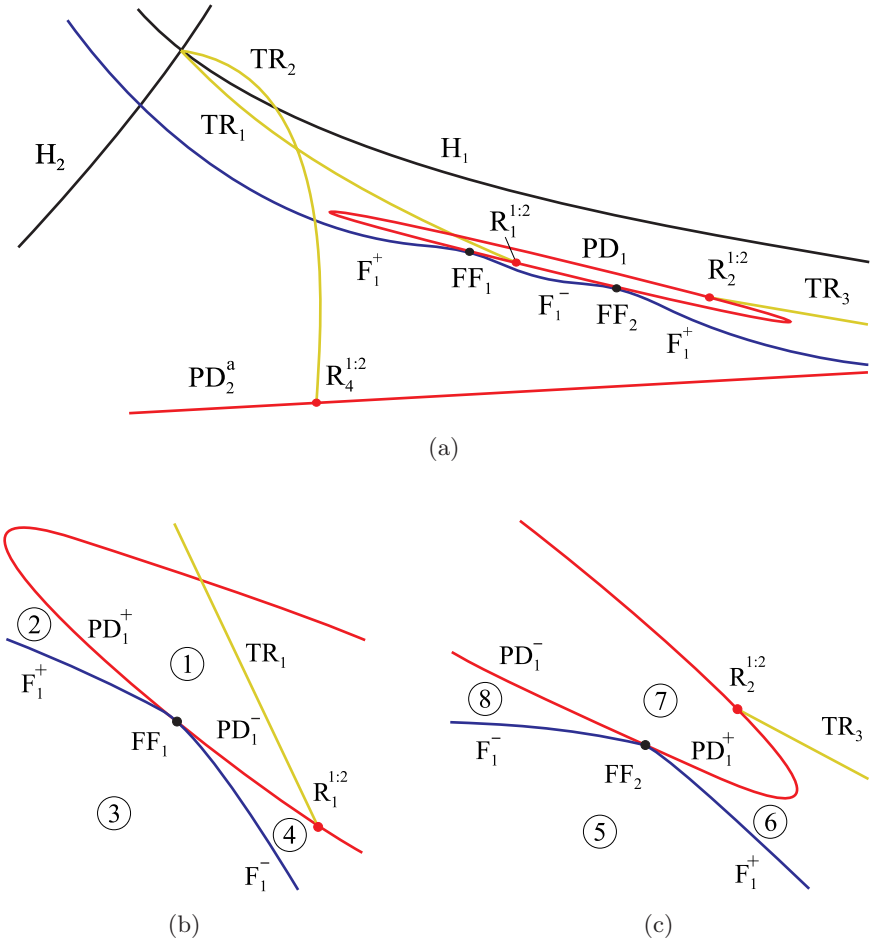

Fig. 18. Schematic representations of the fold-flip bifurcations identified for $\eta_3 = -0.140$.

a period doubling bifurcation crossing PD_1^- back into region 1.

The unfolding of the second fold-flip bifurcation FF_2 is represented schematically in Fig. 18(c) and corresponds to the unfolding of the truncated normal form illustrated in Fig. 6. This case presents a tricky situation because all the limit cycles are saddles or unstable, hence there is always a Floquet multiplier outside the unit circle. This multiplier represents an unstable manifold that does not participate in the fold-flip bifurcation. This fact may be verified making continuations above and below the FF_2 bifurcation point (as close as possible) with η_2 fixed, and checking that there is a multiplier over the real axis smaller than -1, which is virtually fixed before and after the bifurcations $F_1^\pm$ and $PD_1^\pm$. Therefore, if this multiplier is not taken into account in the unfolding of FF_2 it may be seen that, on region 5 there is a saddle period doubling orbit. Crossing F_1^+ a saddle cycle and an unstable orbit connected to the period-two limit cycle, appear on region 6. After passing the curve PD_1^+, the period doubling disappears and the unstable cycle becomes a saddle orbit on region 7. On region 8, one of the saddle cycles suffers a period doubling bifurcation after crossing PD_1^-, so the cycle becomes stable and an unstable period-two orbit is created. The stable orbit and the saddle cycle collapse with each other because of the cyclic fold bifurcation F_1^-, and the unstable period doubling orbit stands alone on region 5.

It is worth to mention that the period-two cycles born at $PD_1^\pm$ suffer bifurcations that are not included in Figs. 17 and 18. More specifically, period-two cyclic fold curves are detected. These bifurcations change the curvature of the cycles emerging from $PD_1^\pm$ and pave the way for the different scenarios surrounding FF_1 and FF_2.

7. Concluding Remarks

In this paper, four bifurcation diagrams associated to the truncated normal form of the nonresonant Hopf-Hopf bifurcation on a coupled electric circuit have been presented. In all cases, the unfolding of

the singularity has been performed numerically considering the variation of two parameters. A third parameter has been used in order to accomplish the transitions among the different diagrams. There have been shown three simple cases and one complex case corresponding to the truncated normal form of the Hopf-Hopf bifurcation. Evidence of the existence of quasi-periodic oscillations involving the interaction of three frequencies, phenomenon known as 3D torus, has been found. The transition between the "simple" case (c) and the "complex" case (d) is due to a change in the stability index of one of the Hopf bifurcation curves. Although it has not been included in this work, this situation may be detected by doing a local analysis of the Hopf bifurcation, and thus alerting about the appearance of this phenomenon. Furthermore, a complex situation of a fold-flip bifurcation of periodic solutions is detected close to the Hopf-Hopf bifurcation. The fold-flip bifurcation has been studied in detail very recently and its appearance seems to be unusual. To our knowledge, this paper is the first to show fold-flip bifurcations close to a Hopf-Hopf bifurcation and thus a gallery of resonance points, folds and cusps of period solutions surrounds these degeneracies.

Acknowledgments

The authors appreciate the financial support of UNS (PGI 24K/30), ANPCyT (PICT 11-12524) and CONICET (PIP 5032).

References

Balanov, A. G., Janson, N. B. & Schöll, E. [2005] "Delayed feedback control of chaos: Bifurcation analysis," *Phys. Rev. E* **71**, 016222–1, 9.

Chamara, P. A. & Coller, B. D. [2004] "A study of double flutter," *J. Fluids Struct.* **19**, 863–879.

Coller, B. D. [2003] "Intriguing nonlinear dynamics of a controller with a sluggish actuator," *Automatica* **39**, 2049–2058.

Gattulli, V., Di Fabio, F. & Luongo, A. [2003] "One to one resonant double Hopf bifurcation in aeroelastic oscillators with tuned mass dampers," *J. Sound Vibr.* **262**, 201–217.

Gordillo, F., Salas, F., Ortega, R. & Aracil, J. [2002] "Hopf bifurcation in indirect field-oriented control of induction motors," *Automatica* **38**, 829–835.

Gu, G., Sparks, A. & Banda, S. S. [1999] "An overview of rotating stall and surge control of axial flow compressors," *IEEE Trans. Contr. Syst. Technol.* **7**, 639–647.

Guckenheimer, J. & Holmes, P. [1993] *Nonlinear Oscillations, Dynamical Systems, and Bifurcations of Vector Fields* (Springer Verlag, NY).

Hassard, B., Kazarinoff, N. & Wan, Y.-H. [1981] *Theory and Applications of Hopf Bifurcation* (Cambridge University Press, London).

Itovich, G. R. & Moiola, J. L. [2005] "Double Hopf bifurcation analysis using frequency domain methods," *Nonlin. Dyn.* **39**, 235–258.

Kuznetsov, Y. A. [1995] *Elements of Applied Bifurcation Theory* (Springer-Verlag, NY).

Kuznetsov, Y. A., Meijer, H. G. E. & van Veen, L. [2004] "The fold-flip bifurcation," *Int. J. Bifurcation and Chaos* **14**, 2253–2282.

LeBlanc, V. G. [2000] "On some secondary bifurcations near resonant Hopf-Hopf interactions," *Dyn. Contin. Discr. Impuls. Syst.* **7**, 405–427.

Liaw, D. C. & Abed, E. H. [1990] "Stabilization of tethered satellites during station keeping," *IEEE Trans. Autom. Contr.* **35**, 1186–1196.

Marsden, J. & McCracken, M. [1976] *Hopf Bifurcation and its Applications* (Springer-Verlag, NY).

Mohamed, A. M. & Emad, F. P. [1993] "Nonlinear oscillations in magnetic bearing systems," *IEEE Trans. Autom. Contr.* **38**, 1242–1245.

Schilder, F., Vogt, W., Schreiber, S. & Osinga, H. [2006] "Fourier methods for quasiperiodic oscillations," *Int. J. Numer. Meth. Engin.* **67**, 629–671.

Wieczorek, S., Krauskopf, B. & Lenstra, D. [2001] "Unnested islands of period doublings in an injected semiconductor laser," *Phys. Rev. E* **64**, 056204–1, 9.

Wieczorek, S., Krauskopf, B., Simpson, T. B. & Lenstra, D. [2005] "The dynamical complexity of optically injected semiconductor lasers," *Phys. Rep.* **416**, 1–128.

Yu, P. [2002] "Analysis on double Hopf bifurcation using computer algebra with the aid of multiple scales," *Nonlin. Dyn.* **27**, 19–53.